IEEE Access
Multidisciplinary ⋮ Rapid Review ⋮ Open Access Journal

Received 9 August 2024, accepted 6 September 2024, date of publication 10 September 2024,
date of current version 19 September 2024.

Digital Object Identifier 10.1109/ACCESS.2024.3457428

APPLIED RESEARCH

Identification of Magnetization Inductance for Six-Phase Induction Machines Driven by Modulated Predictive Control in Field Weakening Zone

MAGNO AYALA[1], JESÚS DOVAL-GANDOY[2], (Member, IEEE), JORGE RODAS[1], (Senior Member, IEEE), OSVALDO GONZALEZ[1], LARIZZA DELORME[1], PAOLA MAIDANA[1], CHRISTIAN MEDINA[1], AND RAÚL GREGOR[1]

[1]Laboratory of Power Systems and Control, Facultad de Ingeniería, Universidad Nacional de Asunción, Luque 2060, Paraguay
[2]Applied Power Electronics Technology Research Group, Universidad de Vigo, 36310 Vigo, Spain

Corresponding author: Magno Ayala (mayala@ing.una.py)

This work was supported in part by CONACYT through INIC01-35 and the Government of Galicia under Grant GPC-ED431B 2023/12, and in part by the Spanish State Research Agency (AEI) under Project PID2022-136908OB-I00/MCIN/AEI/10.13039/501100011033/FEDER-UE.

ABSTRACT Finite-control-set model predictive control (FCS-MPC) has achieved superiority in managing multiphase induction machines due to its quick dynamic response, control flexibility, and overall good performance. Its advantages, including simplicity, computational efficiency, compensation for system perturbations, and effective handling of multivariable problems, have made it a competitive alternative in various industrial applications. Nevertheless, FCS-MPC has some limitations. It is highly dependent on the accuracy of the predictive model's parameters. Unfortunately, the estimation of magnetizing inductance, the most critical factor, especially in the weakening field region, has not been studied yet. Focusing on this gap, this article proposes a technique to estimate the magnetizing inductance in the field weakening zone for a six-phase asymmetrical induction machine driven by the FCS-MPC. Experimental tests have verified the effectiveness of the proposed method, considering stator currents and rotor speed tracking, as well as a reduction in the $(x - y)$ currents.

INDEX TERMS Field weakening operation, magnetizing inductance, multiphase induction machine, predictive current control, space vector modulation.

I. INTRODUCTION

Scientists and industrialists are showing increasing interest in multiphase machines due to their intrinsic characteristics, including fault tolerance, lower current per phase, lower torque ripple and better harmonic profile, compared to their three-phase equivalents [1], [2], [3], [4]. This is why practical applications of multiphase motor drives are becoming more popular in recent years. Koenigsegg's dark matter electric vehicle and the General Electric motor for ship propulsion system are good examples of multiphase machines commercial applications [5], [6].

The most commonly used controls for multiphase machines are generally based on techniques developed for their three-phase equivalents, such as field-oriented control (FOC) based on internal proportional-integral (PI) current control or direct torque control [7], [8], [9]. However, a technique called finite control set model predictive control (FCS-MPC) has been proposed recently, replacing internal current loops. This has become one of the most studied controllers for its intuitive nature, ease of implementation in digital systems and fast transient response compared

The associate editor coordinating the review of this manuscript and approving it for publication was Ning Kang.

to non-linear controllers [10], [11], [12], [13]. Accurate estimation of the parameters of electric machines is required to implement FCS-MPC effectively. In [14], [15], different techniques are observed to estimate the parameters in permanent magnet synchronous motors and [16] and [17] for induction motors. FCS-MPC offers certain advantages, such as handling multiple objectives and constraints, adaptation to different power converters and machine models, and controlling linear and nonlinear systems. Variants of the FCS-MPC have been designed to address its limitations, such as $(x - y)$ current reduction [18], [19], [20], [21], computational load reduction [18], [19], [20], [21], and steady-state error in the $(d - q)$ plane [22], [23], [24], [25].

Specifically, research in [26] demonstrated that the steady-state error for a six-phase asymmetrical induction machine (SPAIM) was corrected, including in the field weakening (FW) zone where the error increases. However, one limitation of the FCS-MPC is its sensitivity to the variation of parameters since this control depends on the mathematical model's precision. Particularly in the FW zone, the magnetization inductance varies given the operating conditions, so the quality of control decreases. Some works made approximations of the magnetization inductance with a polynomial dependent on the current i_{ds} and the current i_m in FW operations [27], [28]. Nonetheless, there is currently no proposed method for accurately determining the magnetization inductance in the flux-weakening zone for multiphase machines under FCS-MPC control.

Therefore, this article proposes a method to estimate the magnetizing inductance in the FW zone for the SPAIM controlled by the FCS-MPC, named PMPC [29]. The controller, which uses different estimated values of the magnetizing inductance, is evaluated through experimental results. The results will be discussed regarding the $(\alpha - \beta)$ currents and rotor speed tracking, $(x-y)$ currents reduction by considering the mean square error (MSE) as figures of merit.

The rest of this document is organized as follows: The SPAIM mathematical model is shown in Section II. Section III presents the proposed controller, including the FCS-MPC design, as a predictive current control (PCC). Section III also describes the design of the PMPC, including an FW algorithm, the steady-state regulator, and the magnetizing inductance estimator. The experimental results show the steady-state and transient behaviour for the proposed technique, where the figures of merit are discussed in Section IV. Finally, the conclusions are defined in Section V.

II. SPAIM MATHEMATICAL MODEL

The FCS-MPC is designed by considering the mathematical model of the system, comprising a SPAIM supplied by a six-phase Voltage Source Inverter (VSI) connected to a DC source, as presented in Figure 1. Accordingly, a continuous representation of the SPAIM is written using differential equations. To reduce the six-phase dimensional space of the system (a, b, c, d, e, f), the vector space decomposition

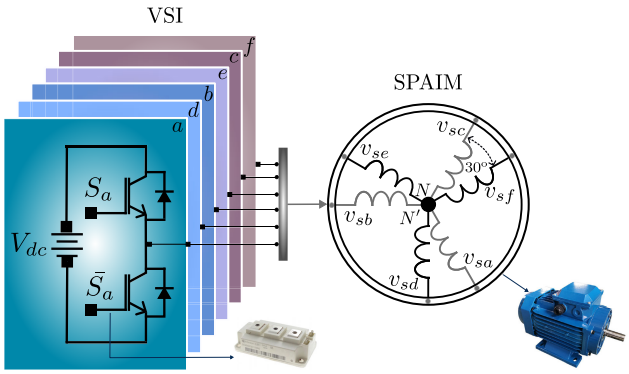

FIGURE 1. SPAIM powered by a six-phase VSI.

(VSD) method is performed, which converts it into three two-dimensional orthogonal planes in the stationary frame references depicted as $(\alpha - \beta)$, $(x - y)$ and $(z_1 - z_2)$, using (1) and the invariant amplitude criterion [30]. At the same time, the SPAIM has a phase shift of 30° between the three-phase windings, and they also have an isolated neutral connection; thus, it is confirmed that the currents $(z_1 - z_2)$ are null. The VSD method is significant in current profiles. Particularly, the $(\alpha - \beta)$ currents are related to the electromechanical energy conversion of the SPAIM. The $(x - y)$ currents mainly contribute to the SPAIM losses and do not produce any torque. This distinction between these two currents enhances the understanding and interpretation of the SPAIM operation and simplifies the implementation of PMPC for improved performance.

$$\mathbf{T} = \frac{1}{3}\begin{array}{c} \begin{matrix} a & d & b & e & c & f \end{matrix} \\ \begin{bmatrix} 1 & \frac{\sqrt{3}}{2} & -\frac{1}{2} & -\frac{\sqrt{3}}{2} & -\frac{1}{2} & 0 \\ 0 & \frac{1}{2} & \frac{\sqrt{3}}{2} & \frac{1}{2} & -\frac{\sqrt{3}}{2} & -1 \\ 1 & -\frac{\sqrt{3}}{2} & -\frac{1}{2} & \frac{\sqrt{3}}{2} & -\frac{1}{2} & 0 \\ 0 & \frac{1}{2} & -\frac{\sqrt{3}}{2} & \frac{1}{2} & \frac{\sqrt{3}}{2} & -1 \\ 1 & 0 & 1 & 0 & 1 & 0 \\ 0 & 1 & 0 & 1 & 0 & 1 \end{bmatrix} \begin{matrix} \alpha \\ \beta \\ x \\ y \\ z_1 \\ z_2 \end{matrix} \end{array} \tag{1}$$

The six-phase VSI, consisting of two isolated gate bipolar transistors (IGBT) per phase, has a discrete nature with $2^6 = 64$ possible switching outputs. The different switching states and the DC source define the output voltages. The 64 different voltages, according to the VSD method, are depicted in Figure 2 in which only 49 vectors (48 vectors + 1 null vector) are considered different in $(\alpha - \beta)$ and $(x - y)$ planes. Hence, the state-space mathematical model of the SPAIM can be presented as follows:

$$\dot{\mathbf{X}}_{(t)} = \mathbf{A}_{(t)}\,\mathbf{X}_{(t)} + \mathbf{B}_{(t)}\,\mathbf{U}_{(t)} + \mathbf{H}\,\varpi_{(t)} \tag{2}$$

where $\mathbf{X}_{(t)} = [x_1, x_2, x_3, x_4, x_5, x_6]^T$ is the state vector representing stator and rotor currents $x_1 = i_{\alpha s}$, $x_2 = i_{\beta s}$, $x_3 = i_{xs}$, $x_4 = i_{ys}$, $x_5 = i_{\alpha r}$ and $x_6 = i_{\beta r}$, $\mathbf{U}_{(t)} = [u_1, u_2, u_3, u_4]^T = [v_{\alpha s}, v_{\beta s}, v_{xs}, v_{ys}]^T$ is the input voltage

vector to power the SPAIM, $\mathbf{H}$ is defined as the noise weight matrix, the process noise is $\varpi_{(t)}$ and $\mathbf{A}_{(t)}$ and $\mathbf{B}_{(t)}$ are matrices defined by the SPAIM parameters as shown:

$$\mathbf{A}_{(t)} = \begin{bmatrix} -R_s c_2 & c_4 L_m \omega_r & 0 & 0 & c_4 R_r & c_4 L_r \omega_r \\ c_4 L_m \omega_r & -R_s c_2 & 0 & 0 & c_4 L_r \omega_r & c_4 R_r \\ 0 & 0 & -R_s c_3 & 0 & 0 & 0 \\ 0 & 0 & 0 & -R_s c_3 & 0 & 0 \\ R_s c_4 & -c_5 L_m \omega_r & 0 & 0 & -c_5 R_r & -c_5 L_r \\ -c_5 L_m \omega_r & R_s c_4 & 0 & 0 & -c_5 L_r & -c_5 R_r \end{bmatrix}$$

$$\mathbf{B}_{(t)} = \begin{bmatrix} c_2 & 0 & 0 & 0 \\ 0 & c_2 & 0 & 0 \\ 0 & 0 & c_3 & 0 \\ 0 & 0 & 0 & c_3 \\ -c_4 & 0 & 0 & 0 \\ 0 & -c_4 & 0 & 0 \end{bmatrix}$$

where R_s, R_r, L_m (mutual inductance), $L_r = L_{lr} + L_m$ and $L_s = L_{ls} + L_m$ are the electrical parameters of the SPAIM. The coefficients are $c_1 = L_s L_r - L_m^2$, $c_2 = \frac{L_r}{c_1}$, $c_3 = \frac{1}{L_{ls}}$, $c_4 = \frac{L_m}{c_1}$ and $c_5 = \frac{L_s}{c_1}$.

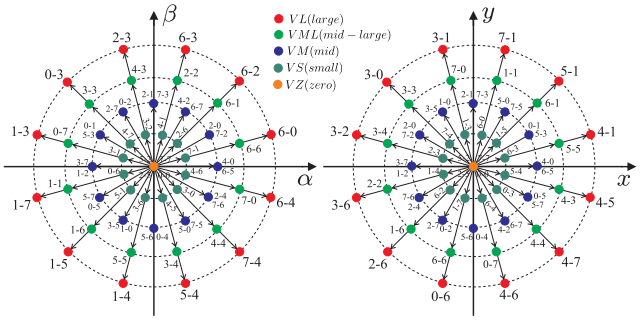

FIGURE 2. Voltage space vectors and 64 switching states in ($\alpha - \beta$) and ($x - y$) planes for the SPAIM.

A simple mathematical model for the VSI is presented to ensure an effective optimization calculation. Stator voltages are related on the switching state $\mathbf{S}$, where $\mathbf{S} = [S_a, S_d, S_b, S_e, S_c, S_f]$, $\mathbf{S}_i \in \{0, 1\}$ and can be obtained from the six-phase VSI model $\mathbf{M}_{[\mathbf{S}]}$ presented:

$$\mathbf{M}_{[\mathbf{S}]} = \frac{1}{3} \begin{bmatrix} 2 & 0 & -1 & 0 & -1 & 0 \\ 0 & 2 & 0 & -1 & 0 & -1 \\ -1 & 0 & 2 & 0 & -1 & 0 \\ 0 & -1 & 0 & 2 & 0 & -1 \\ -1 & 0 & -1 & 0 & 2 & 0 \\ 0 & -1 & 0 & -1 & 0 & 2 \end{bmatrix} \mathbf{S}^T \tag{3}$$

The six-phase VSI generates a voltage in every phase through the switching signals, and then they are transformed to ($\alpha - \beta$) and ($x - y$) planes. They are presented as $\mathbf{U}_{(t)}$:

$$\mathbf{U}_{(t)} = V_{dc}\, \mathbf{T}\, \mathbf{M}_{[\mathbf{S}]}. \tag{4}$$

where V_{dc} is the DC source. The output vector, $\mathbf{Y}$, is:

$$\mathbf{Y}_{(t)} = \mathbf{C}\, \mathbf{X}_{(t)} + \nu_{(t)} \tag{5}$$

where $\nu_{(t)}$ is the measurement noise and

$$\mathbf{C} = \begin{bmatrix} 1 & 0 & 0 & 0 & 0 & 0 \\ 0 & 1 & 0 & 0 & 0 & 0 \\ 0 & 0 & 1 & 0 & 0 & 0 \\ 0 & 0 & 0 & 1 & 0 & 0 \end{bmatrix}.$$

The SPAIM torque is calculated through these equations:

$$T_e = 3\, P \left(\psi_{\alpha s} i_{\beta s} - \psi_{\beta s} i_{\alpha s}\right) \tag{6}$$

$$J_i\, \dot{\omega}_m + B_i\, \omega_m = (T_e - T_L) \tag{7}$$

$$\omega_r = P \omega_m \tag{8}$$

where T_e is the electromagnetic torque, $\psi_{\alpha s}$ and $\psi_{\beta s}$ are the stator fluxes, P the number of pole pairs, B_i the friction coefficient, J_i is the inertia coefficient, T_L is the load torque, ω_r and ω_m are the rotor mechanical speed and the rotor electrical angular speed respectively.

III. CONTROL SCHEME APPLIED TO THE SPAIM

This section illustrates the complete control scheme which includes a speed control, an inner PCC with a reduced-order observer, the defined cost function, the modulation stage, the FW operation, the steady-state current regulator and the estimation of the magnetizing inductance on the FW zone.

A. OUTER SPEED CONTROL

The SPAIM mechanical speed outer loop is designed based on a PI controller with a saturated output and an anti-windup method, as proposed in [31]. This PI is selected due to its simplicity and robustness. The PI speed regulator generates the dynamic current reference named i_{qs}^*.

At the same time, the slip frequency (ω_{sl}) calculation is developed based on the indirect rotor field-oriented control (IRFOC) method through the ($d-q$) stator current references (i_{ds}^*, i_{qs}^*) and the rotor parameters R_r, L_r. The speed control is defined as follows:

$$i_{qs}^* = K_p(\omega_m^* - \omega_m) + \frac{K_i(\omega_m^* - \omega_m)}{z - 1} \tag{9}$$

where K_p and K_i are the PI parameters representing the proportional and integral parts, respectively.

B. PCC BASED ON PMPC

To the PMPC to perform correctly, the SPAIM ((2) and (5)) needs to be defined into a discrete form, and for this case, a direct Euler method is applied to reduce computational complexity. The equations will be suitable for digital processing, where predicted variables are obtained from past values. Thus, the prediction of the variables, defined as $\hat{\mathbf{X}}_{[k+1|k]}$, is calculated:

$$\hat{\mathbf{X}}_{[k+1|k]} = \mathbf{X}_{[k]} + \mathrm{f}\left(\mathbf{X}_{[k]},\ \mathbf{U}_{[k]},\ T_s,\ \omega_{r[k]}\right) \tag{10}$$

where $[k]$ is the present sample, f is the function symbol and T_s the sampling time.

C. REDUCED ORDER OBSERVERS

In the presented model (2), only the stator currents and the rotor speed can be measured [32]. The stator voltages are obtained from the switching states for the six-phase VSI. However, the rotor currents cannot be measured, so they must be observed. This can be done through reduced-order observers. Some methods like the Luenberger Observer (LO) and Kalman Filter (KF) were proposed [33], where the KF is considered a better selection as the observer gains are updated through the consideration of the noise input to the sensors. For a comprehensive understanding of the dynamics and error convergence of the KF, refer to [34], given that this aspect was omitted from the present work for reasons of conciseness.

D. COST FUNCTION

The cost function is defined from optimising essential variables, such as reduction of torque ripple and the harmonic distortion [21]. However, in current control, the error in the predicted stator currents in the $(\alpha-\beta)$ and $(x-y)$ planes are the most important variables. PMPC calculates the cost function for 49 iterations:

$$J_{[k+2|k]} = \Big[(i^*_{\alpha s[k+2]} - \hat{i}_{\alpha s[k+2|k]})^2 + (i^*_{\beta s[k+2]} - \hat{i}_{\beta s[k+2|k]})^2 + \lambda_{xy}\left((i^*_{xs[k+2]} - \hat{i}_{xs[k+2|k]})^2 + (i^*_{ys[k+2]} - \hat{i}_{ys[k+2|k]})^2\right)\Big]^{\frac{1}{2}} \tag{11}$$

By considering (12), a second step forward prediction of the stator currents $\hat{i}_{s[k+2|k]}$ is performed to compensate dead time [34]. The stator current references are depicted as $i^*_{s[k+2]}$. Weighting factor optimization is a subject of current research interest, with some studies dedicated to exploring this topic [35], [36]. Usually, in multiphase machines, λ_{xy} is tuned to prioritize the $(\alpha-\beta)$ currents.

$$\hat{\mathbf{X}}_{[k+2|k]} = \mathbf{A}_{[k]}\mathbf{X}_{[k+1]} + \mathbf{B}_{[k]}\mathbf{U}_{[k+1]} + \mathbf{H}\varpi_{[k]} \tag{12}$$

E. MODULATION STAGE

PMPC uses a modulation stage designed as a space vector modulation (SVM). PMPC uses 4 vectors, which includes 2 mid vectors (VM) and 2 large vectors (VL). This modulation improves the performance of the stator current tracking by including the adjacent VM per sector to avoid the null vectors (VZ). VZ limits the voltage range of the vectors when combined with its corresponding duty cycle, reducing the PMPC ability to track the stator currents in $(\alpha-\beta)$ plane because VZ duty cycle is increased when the $(x-y)$ currents are reduced [29]. The duty cycles, for the four active vectors d_1, d_2, d_3 and d_4, are obtained by solving these equations:

$$d_1 = \frac{\sigma}{J_1}\; d_2 = \frac{\sigma}{J_2}\; d_3 = \frac{\sigma}{J_3}\; d_4 = \frac{\sigma}{J_4} \tag{13}$$

$$d_1 + d_2 + d_3 + d_4 = 1 \tag{14}$$

where J_1, J_2, J_3 and J_4 are the cost functions (11) for every vector in any sector. σ can be clear and the duty cycles for each vector are defined in the following equations:

$$J_{T1} = J_1J_3J_4 + J_2J_3J_4 \tag{15}$$

$$J_{T2} = J_1J_2J_4 + J_1J_2J_3 \tag{16}$$

$$d_1 = \frac{J_2J_3J_4}{J_{T1}+J_{T2}} \tag{17}$$

$$d_2 = \frac{J_1J_3J_4}{J_{T1}+J_{T2}} \tag{18}$$

$$d_3 = \frac{J_1J_2J_4}{J_{T1}+J_{T2}} \tag{19}$$

$$d_4 = \frac{J_1J_2J_3}{J_{T1}+J_{T2}} \tag{20}$$

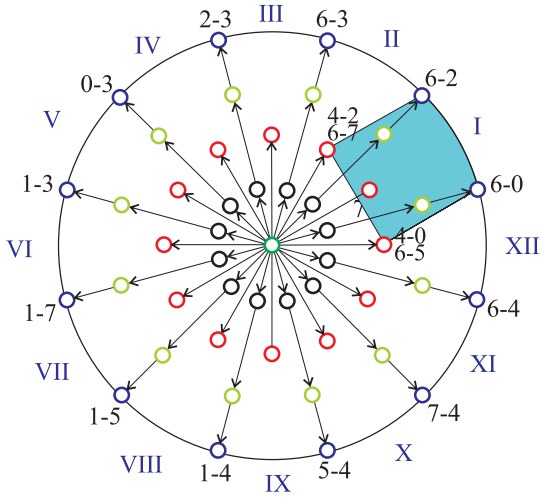

FIGURE 3. Possible sectors of PMPC for the six-phase VSI.

PMPC analyses all the 12 sectors, as presented in Figure 3, by obtaining the cost function for every vector and the duty cycles of each vector are defined with their cost functions. At last, the cost function to select a sector is depicted as:

$$G_{[k+2|k]} = d_1J_1 + d_2J_2 + d_3J_3 + d_4J_4 \tag{21}$$

F. FIELD WEAKENING OPERATION

The simplest method for FW operations is to modify the rotor flux reference in inverse proportion to ω_m [37], reducing the magnetic field. In this method, above rated speed, the reference currents i^*_{ds} and i^*_{qs} are calculated in the next

equations:

$$i^*_{ds} = \frac{\omega_{m(rated)}}{\omega_m} i_{ds(rated)} \tag{22}$$

$$i^*_{qs(max)} = \sqrt{i^2_{s(max)} - i^{*2}_{ds}} \tag{23}$$

where $i_{s(max)}$ is the maximum stator current value, typically limited to 1.5 times the rated current [38]. At the same time, $i^*_{qs(max)}$ is the maximum reference value if an external speed control is not performed. In this case, it is used to limit the output of the speed controller i_{qs}. Usually, when i^*_{ds} is decreased, to achieve the maximum stator current, i^*_{qs} is increased.

G. STEADY-STATE CURRENT REGULATOR

The steady-state current regulator is based on an integrator combined with the PMPC to mitigate the steady-state error in $(d-q)$ currents. This approach involves the following function [39]:

$$I(z) = \frac{K_R z^{-1}}{1 - z^{-1}} \tag{24}$$

PMPC with a small sampling time is approximated to a closed-loop system with eigenvalues at the origin in the complex plane, so it is considered as a delay z^{-1} in the $(d-q)$ plane [39]. Although a limited version of a more complex controller like the MPC, it simplifies the analysis in the $(d-q)$ plane. So, the following open-loop function is defined:

$$G(z) = \frac{K_R z^{-2}}{1 - z^{-1}} \tag{25}$$

At the same time, the close-loop function is:

$$\frac{i_{dqs}(z)}{i_{dqs}(z)^*} = \frac{K_R z^{-2}}{1 - z^{-1} + K_R z^{-2}} \tag{26}$$

where it can be seen that to stay inside the unit circle, $0 < K_R < 1$ must be satisfied. Finally, the output is saturated, and an anti-windup is included to provide more security for the system.

It must be considered that an integrator has a slow response and could present oscillations in its dynamic behaviour. For this reason, a lead compensator (LC) is also included to accelerate the response since it has a high transient response speed and bandwidth. This compensator is typically designed based on some criteria. In this case, the selected criteria is the frequency domain behaviour of the simplified system shown in (25) to obtain an increase of 40° of phase margin, improving the system bandwidth [26]. The compensator is defined as follows:

$$LC(s) = \frac{Ts + 1}{\alpha Ts + 1} \tag{27}$$

being α the attenuation factor, T is the compensator time and s the Laplace operator. Then, its discrete version with a zero-order holder is presented:

$$LC(z) = \frac{\frac{z}{\alpha} + 1 - \frac{1}{\alpha} - e^{-(\frac{T_s}{\alpha T})}}{z - e^{-(\frac{T_s}{\alpha T})}} \tag{28}$$

The parameters for the $(d-q)$ current regulator are defined as: $\alpha = 0.2$, $T = 0.24$, $K_R = 100T_s$. PMPC is finally depicted as a block diagram in Figure 4.

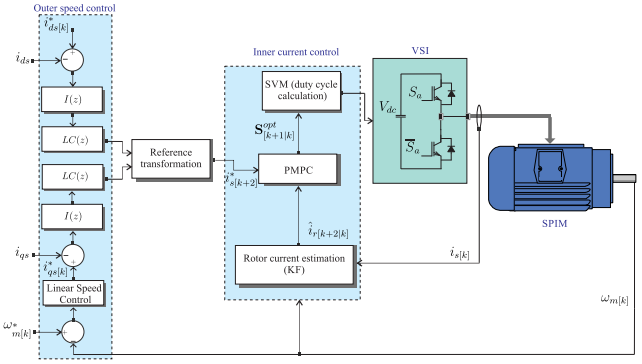

FIGURE 4. Block diagram of PMPC.

H. MAGNETIZING INDUCTANCE IN FIELD WEAKENING ZONE

It is known that the magnetizing inductance may vary when the rotor flux reference changes in the FW zone. Some approximation approaches have been proposed to consider this phenomenon. Most of these approaches are based on polynomial functions dependent on the i_{ds} or the i_m currents [27], [28].

As (22) is used to calculate the i^*_{ds} in FW, the inversely proportional relationship with the rotor speed can be observed. At the same time, an approximation to the behaviour of the magnetization current i_m in FW can be considered, applying the following:

$$i_m = \frac{\omega_{m(rated)}}{\omega_m} i_{m(rated)} \tag{29}$$

Furthermore, the following can be assumed:

$$i_{m(rated)} = \frac{v_{m(rated)}}{x_{m(rated)}} = \frac{v_{m(rated)}}{2\pi f_{(rated)} L_{mag(rated)}} \tag{30}$$

$$i_m = \frac{v_{m(rated)}}{x_m} = \frac{v_{m(rated)}}{2\pi f L_{mag}} \tag{31}$$

Substituting (30) and (31) into (29)

$$L_{mag} = \frac{L_{mag(rated)} f_{(rated)} \omega_m}{f\, \omega_{m(rated)}} \tag{32}$$

$$L_{mag} = \frac{L_{mag(rated)} f_{(rated)} \frac{2\pi f}{P}(1 - Slip)}{f \frac{2\pi f_{(rated)}}{P}(1 - Slip_{(rated)})} \tag{33}$$

At the end of the simplifications, it is obtained:

$$L_{mag} = \frac{L_{mag(rated)}(1 - Slip)}{(1 - Slip_{(rated)})} \tag{34}$$

Considering the approximation of the Slip within the IRFOC, it can be calculated below:

$$Slip = \frac{i^*_{qs}}{i^*_{ds}} \frac{R_r}{L_r} \frac{1}{\omega_s} \tag{35}$$

$$Slip = \frac{i^*_{qs}}{i^*_{ds}} \frac{R_r}{(3L_{mag(rated)} + L_{lr})} \frac{1}{\omega_s} \tag{36}$$

Applying (36) in (34)

$$L_{mag} = \frac{1}{(1 - Slip_{(rated)})} (L_{mag(rated)} \tag{37}$$

$$- L_{mag(rated)} \frac{i^*_{qs}}{i^*_{ds}} \frac{R_r}{(3L_{mag(rated)} + L_{lr})} \frac{1}{\omega_s}) \tag{38}$$

Since $3L_{mag(rated)} + L_{lr} \approx 3L_{mag(rated)}$ and $\omega_s = 2\pi f$ the equation can be simplified

$$L_{mag} = \frac{1}{(1 - Slip_{(rated)})} (L_{mag(rated)} - \frac{i^*_{qs}}{i^*_{ds}} \frac{R_r}{3} \frac{1}{2\pi f}) \tag{39}$$

Finally, considering that i^*_{ds} varies with the rotor speed according to (22), the proportion of the speeds $\frac{\omega_{m(rated)}}{\omega_m} \approx \frac{f_{(rated)}}{f}$, then:

$$L_{mag} = \frac{1}{(1 - Slip_{(rated)})} (L_{mag(rated)} \tag{40}$$

$$- \frac{i^*_{qs}}{i_{ds(rated)} f_{(rated)}} \frac{R_r}{3} \frac{1}{2\pi}) \tag{41}$$

For a simple visualization, these constants are considered $k_1 = \frac{1}{(1 - Slip_{(rated)})}$, $k_2 = k_1 \frac{1}{i_{ds(rated)} f_{(rated)}} \frac{R_r}{3} \frac{1}{2\pi}$. Then the magnetizing inductance will be affected mainly by i^*_{qs}:

$$L_{mag} = k_1 L_{mag(rated)} - k_2 i^*_{qs} \tag{42}$$

Figure 5 presents the variation in the magnetizing inductance in FW for different values of i^*_{qs} compared to its rated value. k_1 is approximately 1.181 and k_2 is 0.0086.

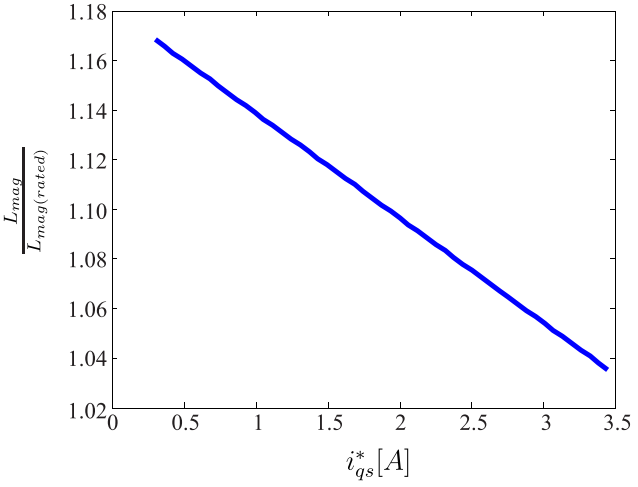

FIGURE 5. Magnetizing inductance (L_{mag}) versus i^*_{qs} current graph.

IV. EXPERIMENTAL RESULTS

To experimentally verify the proposal, tests were carried out with a six-phase drive with the PMPC approach in which the performances of the steady-state and transient regime were compared when the parameter L_m was kept constant and when it was varied according to (42). The experiment includes a SPAIM, two typical three-phase VSIs, and a DC source. The VSIs are activated by a real-time rapid prototyping platform controlled with MATLAB/Simulink 2014a named dSPACE MABXII DS1401. The SPAIM parameters were obtained by AC time domain conventional methods and stand-still tests [40] and are depicted in Table 1.

TABLE 1. SPAIM parameters.

Parameter	Value	Parameter	Value
R_r (Ω)	6.9	R_s (Ω)	6.7
L_s (mH)	654.4	L_r (mH)	626.8
L_m (mH)	614	L_{ls-xy} (mH)	5.3
ω_{m-nom} (rpm)	2 540	P_w (kW)	2
J_i (kg·m^2)	0.07	B_i (kg·m^2/s)	0.0004
P (pole pair)	1	$Slip$	0.1533
T_{e-nom} (Nm)	7.5	i_{s-rms} (A)	2.2

The currents are measured by LA 55-P s sensors. The SPAIM rotor angle is measured by a 1024 ppr incremental encoder, and its speed is estimated from it. At the same time, a mechanical load is performed on the SPAIM using an adjustable 5 HP eddy current brake. At last, a photo of the entire setup is shown in Figure 6.

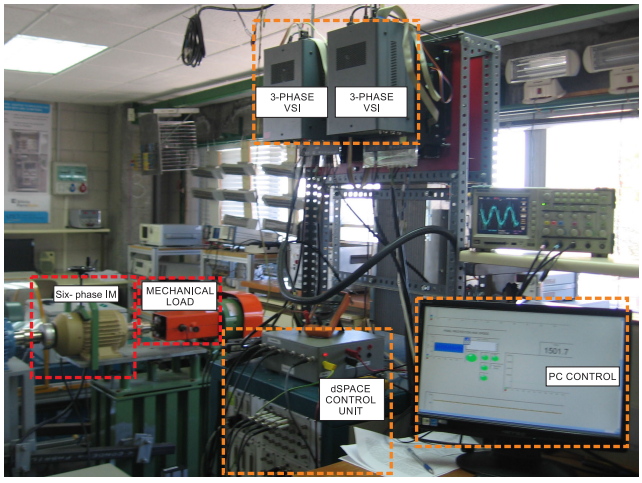

FIGURE 6. Photo of the entire setup, including the SPAIM, the dSPACE platform, the eddy current brake and the two three-phase VSIs.

The cost function in (11) with $\lambda_{xy} = 0.1$ was adjusted to perform the PMPC [29]. The measurement and process noise values are calculated by the autocovariance-least-squared (ALS) method since it provides unbiased estimations with the lowest covariance, guaranteeing an optimal KF

TABLE 2. Performance of stator currents, MSE (A) and MSE (A) for PMPC with constant L_{mag} with $i_{qs} = 1.5$ A at different rotor speeds (rpm).

ω_m^*	MSE_α	MSE_β	MSE_x	MSE_y	MSE_{ω_m}
2150	0.1011	0.1046	0.2385	0.2358	2.0745
2550	0.0917	0.1117	0.2282	0.2345	2.8284
3000	0.1144	0.1170	0.2299	0.2172	5.0697
3400	0.1069	0.1104	0.2198	0.2136	4.5487

TABLE 3. Performance of stator currents, MSE (A) and MSE (A) for PMPC with constant L_{mag} with $i_{qs} = 2.5$ A at different rotor speeds (rpm).

ω_m^*	MSE_α	MSE_β	MSE_x	MSE_y	MSE_{ω_m}
2150	0.1018	0.1013	0.2510	0.2590	2.8162
2550	0.1008	0.1022	0.2548	0.2824	3.2854
3000	0.1059	0.1085	0.2791	0.2503	4.2332
3400	0.0991	0.1042	0.2684	0.2677	4.2882

TABLE 4. Performance of stator currents, MSE (A) and MSE (A) for PMPC with estimated $\hat{L}_{mag}$ with $i_{qs} = 1.5$ A at different rotor speeds (rpm).

ω_m^*	MSE_α	MSE_β	MSE_x	MSE_y	MSE_{ω_m}
2150	0.0983	0.1000	0.2674	0.2638	1.9011
2550	0.0949	0.0976	0.2509	0.2673	3.5485
3000	0.0996	0.1016	0.2650	0.2830	3.0653
3400	0.1066	0.1075	0.2680	0.2706	3.6153

TABLE 5. Performance of stator currents, MSE (A) and MSE (A) for PMPC with estimated $\hat{L}_{mag}$ with $i_{qs} = 2.5$ A at different rotor speeds (rpm).

ω_m^*	MSE_α	MSE_β	MSE_x	MSE_y	MSE_{ω_m}
2150	0.0954	0.0956	0.2237	0.2117	1.7045
2550	0.0978	0.1064	0.2082	0.2364	3.2823
3000	0.0987	0.1172	0.2283	0.2369	2.9812
3400	0.1059	0.1160	0.2213	0.2355	3.9779

adjustment [34]. The applied values are $\hat{Q}_w = 0.0022$ and $\hat{R}_v = 0.0022$. Then, $(x - y)$ current references are fixed to zero ($i_{xs}^* = i_{ys}^* = 0$) since this plane is only related to the SPAIM losses and a fixed d current ($i_{ds}^* = 1$ A) was considered in rated speed conditions. The sampling frequency is set to 16 kHz. At last, for hardware limitations, i.e., the encoder and the eddy current brake top speeds, the DC source is diminished to 65% of the rated value, set to 400 V, and the rated speed in this condition is now 1700 rpm.

A. FIGURES OF MERIT

The proposal is analyzed in steady-state and transient conditions and then evaluated with figures of merit, such as MSE, which is obtained between the reference and measured stator currents in $(\alpha - \beta)$ and $(x - y)$ planes and the rotor

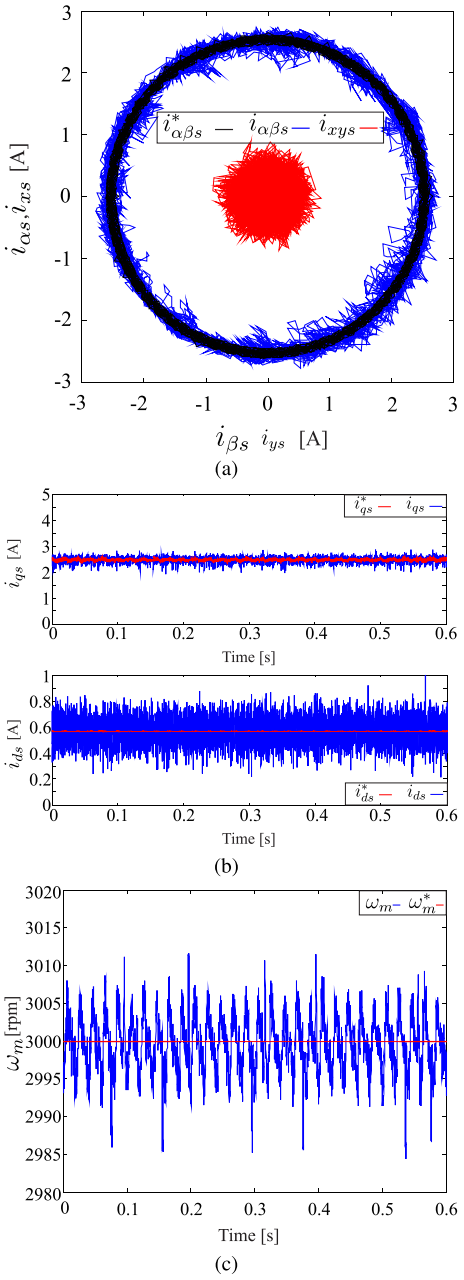

FIGURE 7. Obtained results from the SPAIM at a speed of 2550 rpm and $i_{qs} = 2.5$ A: (a) Polar representation of stator currents; (b) Stator currents i_{ds}, i_{ds}^* and i_{qs}, i_{qs}^*; (c) Rotor speed tracking ω_m and ω_m^*.

speed. The MSE is described:

$$\text{MSE}(i_{s\Phi}) = \sqrt{\frac{1}{N}\sum_{k=1}^{N}(i_{s\Phi}[k] - i_{s\Phi}^*[k])^2} \tag{43}$$

being N the number of samples, $i_{s\Phi}$ the measured stator currents, $i_{s\Phi}^*$ the stator currents reference and $\Phi \in \{\alpha, \beta, x, y\}$.

B. STEADY-STATE RESULTS

The tests in steady-state are performed with different rotor speeds: 2150 rpm, 2550 rpm, 3000 rpm and 3400 rpm. Table 2

and 3 show the results for all rotor speeds for the PMPC with constant L_{mag} with $i_{qs} = 1.5$ A and $i_{qs} = 2.5$ A, respectively. Also, in Table 4 and 5, the results with the estimated $\hat{L}_{mag}$ with the same $i_{qs} = 1.5$ A and $i_{qs} = 2.5$ A are shown. Some of them are the MSE of the rotor speed and the stator currents at $(\alpha - \beta)$ and $(x - y)$ planes.

Figure 7 presents the stator currents tracking in $(d - q)$ planes for PMPC, a polar representation of the stator currents in the $(\alpha - \beta)$ and $(x - y)$ planes and the rotor speed tracking for a speed of 2550 rpm. Tests were performed with a fixed eddy current to establish a constant mechanical load that generates a i_{qs} current of 2.5 A. At the same time, Figure 8 shows the six-phase stator currents in steady-state regime.

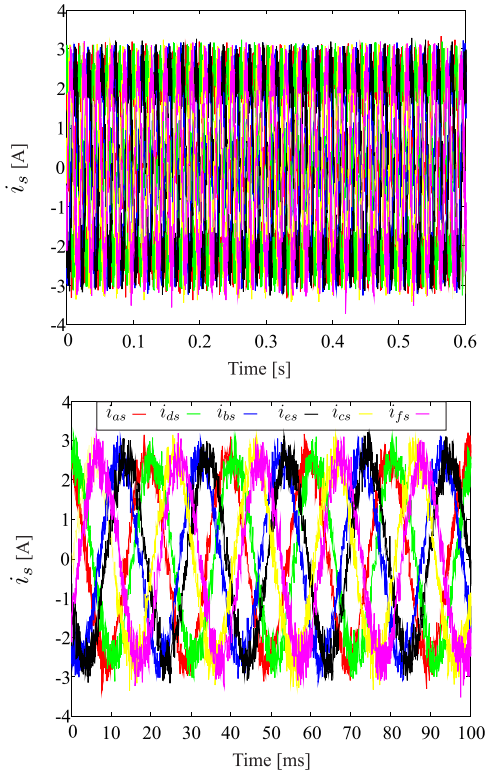

FIGURE 8. Obtained results from the SPAIM at a speed of 2550 rpm and $i_{qs} = 2.5$ A: Six-phase stator currents.

C. TRANSIENT RESULTS

For the transient analysis, two tests are presented: a step change in mechanical speed, from 2550 to 3300 rpm and a step change in the mechanical load that generates a step change in q current from 0.25 to 3 A for PMPC with constant L_{mag} and with the estimated $\hat{L}_{mag}$. Figures 9 and 10 present the dynamic behaviour which includes the i_{qs} dynamic response and the rotor speed ω_m. Table 6 depict the values for the figures of merit under those transient conditions.

D. DISCUSSION

To perform a comparative analysis, the obtained MSE with the constant L_{mag} and estimated $\hat{L}_{mag}$ were taken into account.

TABLE 6. Performance of stator q current, MSE (A) and rotor speed MSE (rpm) for PMPC for the step change of speed and torque load.

Constant L_{mag}		
Step change	**MSEq**	**MSE$_{\omega_m}$**
Speed (2550 to 3300 rpm)	0.1117	266.11
Torque load (0.25 to 3.5 Nm)	0.0956	118.34
Estimated $\hat{L}_{mag}$		
Step change	**MSEq**	**MSE$_{\omega_m}$**
Speed (2550 to 3300 rpm)	0.1075	253.26
Torque load (0.25 to 3.5 Nm)	0.0970	96.54

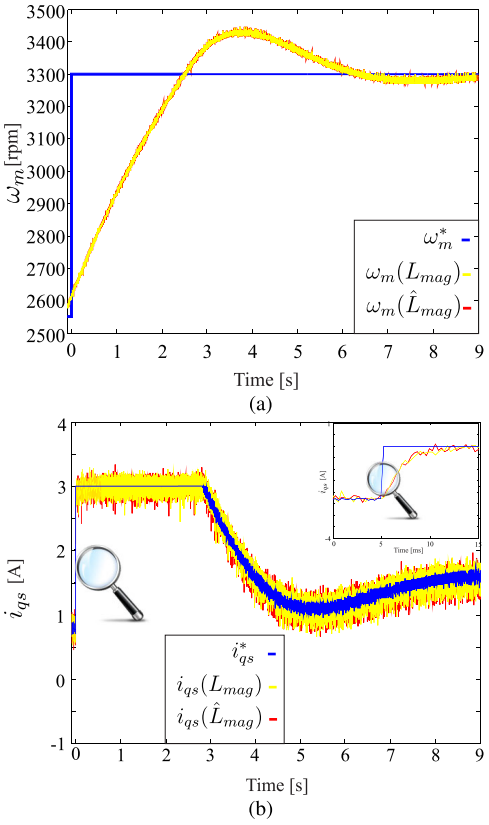

FIGURE 9. Transient response of stator currents (i_{qs}) and the rotor speed (ω_m) from a speed step response of 2550 to 3300 rpm: (a) ω_m; (b) i_{qs}.

To do this, the following equation is considered in terms of %:

$$MSE_{reduction} = 100\frac{MSE_{[L_{mag}]} - MSE_{[\hat{L}_{mag}]}}{MSE_{[L_{mag}]}} \tag{44}$$

If the result is positive, it means that the performance worsened; if it is negative, it means that it improved since it represents the percentage reduction of the MSE for the proposal.

The experimental results reveal that the estimated $\hat{L}_{mag}$ has led to notable improvements in specific performance aspects of the SPAIM, as shown in Figure 11. Three scenarios can be seen, two in steady-state for different speeds and

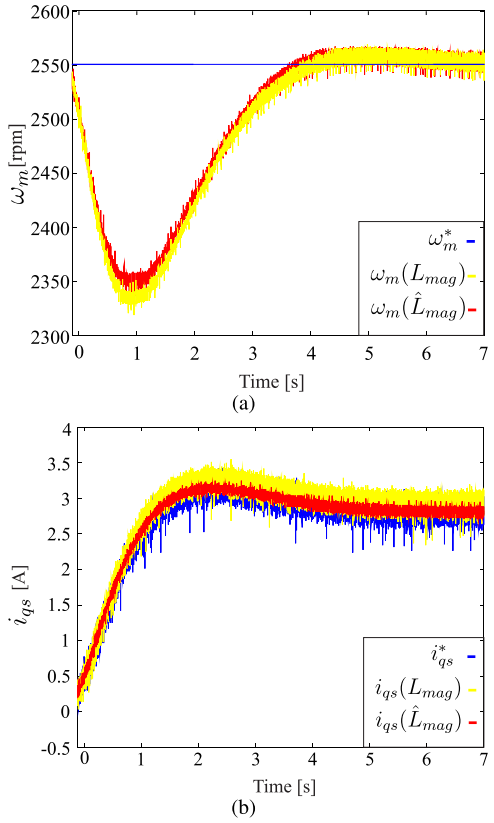

FIGURE 10. Transient response of stator currents (i_{qs}) and the rotor speed (ω_m) from a step change in mechanical load that generates a step change in i_{qs} current from 0.25 to 3 A: (a) ω_m; (b) i_{qs}.

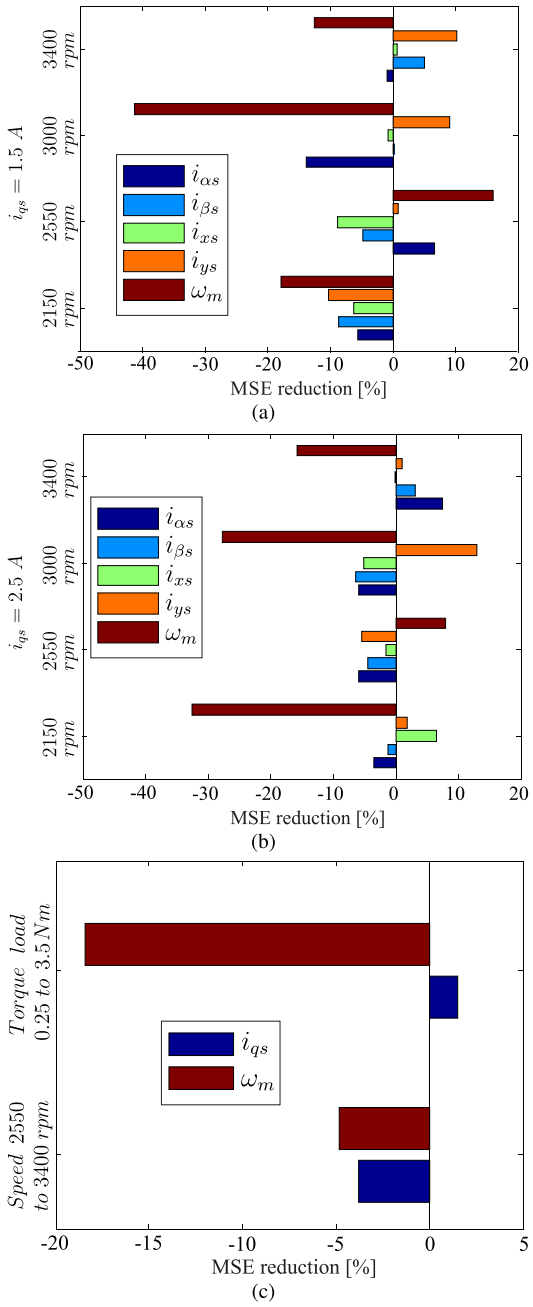

FIGURE 11. Comparison of MSE between constant L_{mag} and estimated $\hat{L}_{mag}$ for different conditions: (a) Steady-state results with $i_{qs} = 1.5$ A; (b) Steady-state results with $i_{qs} = 2.5$ A; (c) Transient results with step change of speed and torque.

i_{qs} current and one for transient analysis with change in speed and load torque. Regarding the steady-state operation, it can be seen that there are varied results for both scenarios. A better performance is obtained for some parameters; in others, it is not. However, it can be verified that there is more reduction of MSE at more operating points, especially in the case of mechanical speed tracking, and the adverse results do not have a very high value compared to those that are reduced.

The slight variations in MSE, less than 10%, are deemed negligible, considering the inherent variability observed in figures of merit, which can fluctuate between trials due to temperature and measurement errors [41]. Therefore, despite minor adverse results, the overall improvement in transient analysis, particularly in speed tracking, underscores the effectiveness of the proposed approach.

Considering other proposals in the literature, approximations of the L_m have been found considering the stator current i_{ds} [27] and the magnetizing current i_m [28]. In the first case, considering a qualitative approach, the results showed a significant improvement in the transient response speed. In the second case, tests were observed in sensorless speed control, which, with the estimation, significantly improves the speed tracking in a steady-state regime, although, in a transient regime, it presents a slower behaviour.

V. CONCLUSION

The main objective of this article is to estimate the magnetization inductance in the field weakening zone. An estimation method was obtained for said inductance concerning its nominal value and the current i_{qs}, which depends directly on the load torque. Experimental tests were then carried out, which validated the estimated $\hat{L}_{mag}$ for a constant L_{mag}. The results confirmed better performance in most operating points, especially in transient conditions,

speed, and load torque. The estimation method is carried out online, but the computational cost is minimal since it is a first-degree equation dependent on SPAIM parameters. It is worth mentioning that although there are several proposals in the literature on estimating the L_m, no approach has yet approximated it based on the stator current i_{qs}, which depends on the motor load torque and is constantly varied during a typical operation.

REFERENCES

[1] F. Barrero and M. J. Duran, "Recent advances in the design, modeling, and control of multiphase machines—Part I," *IEEE Trans. Ind. Electron.*, vol. 63, no. 1, pp. 449–458, Jan. 2016.

[2] M. J. Duran and F. Barrero, "Recent advances in the design, modeling, and control of multiphase machines—Part II," *IEEE Trans. Ind. Electron.*, vol. 63, no. 1, pp. 459–468, Jan. 2016.

[3] E. Levi, "Advances in converter control and innovative exploitation of additional degrees of freedom for multiphase machines," *IEEE Trans. Ind. Electron.*, vol. 63, no. 1, pp. 433–448, Jan. 2016.

[4] X. Peng, Z. Liu, and D. Jiang, "A review of multiphase energy conversion in wind power generation," *Renew. Sustain. Energy Rev.*, vol. 147, Sep. 2021, Art. no. 111172.

[5] K. A. Ab. (2023). *Here's How Koenigsegg's 'Dark Matter' Electric Motor Makes 800 Hp*. [Online]. Available: https://www.thedrive.com/news/heres-how-koenigseggs-dark-matter-electric-motor-makes-800-hp

[6] G. Vernova. (2020). *Ge Powers Us Navy's 1st Full-electric Power and Propulsion Ship*. [Online]. Available: https://www.gevernova.com/power-conversion/news/ge-powers-us-navys-1st-full-electric-power-and-propulsion-ship

[7] Z. Liu, Y. Li, and Z. Zheng, "A review of drive techniques for multiphase machines," *CES Trans. Electr. Mach. Syst.*, vol. 2, no. 2, pp. 243–251, Jun. 2018.

[8] I. G. Prieto, M. J. Duran, P. Garcia-Entrambasaguas, and M. Bermudez, "Field-oriented control of multiphase drives with passive fault tolerance," *IEEE Trans. Ind. Electron.*, vol. 67, no. 9, pp. 7228–7238, Sep. 2020.

[9] U. R. Muduli, R. K. Behera, K. Al Hosani, and M. S. E. Moursi, "Direct torque control with constant switching frequency for three-to-five phase direct matrix converter fed five-phase induction motor drive," *IEEE Trans. Power Electron.*, vol. 37, no. 9, pp. 11019–11033, Sep. 2022.

[10] J. Rodriguez, M. P. Kazmierkowski, J. R. Espinoza, P. Zanchetta, H. Abu-Rub, H. A. Young, and C. A. Rojas, "State of the art of finite control set model predictive control in power electronics," *IEEE Trans. Ind. Informat.*, vol. 9, no. 2, pp. 1003–1016, May 2013.

[11] J. Rodriguez et al., "Latest advances of model predictive control in electrical drives—Part I: Basic concepts and advanced strategies," *IEEE Trans. Power Electron.*, vol. 37, no. 4, pp. 3927–3942, Apr. 2022.

[12] M. Mamdouh and M. A. Abido, "Simple predictive current control of asymmetrical six-phase induction motor with improved performance," *IEEE Trans. Ind. Electron.*, vol. 70, no. 8, pp. 7580–7590, Aug. 2023.

[13] M. J. Duran, I. Gonzalez-Prieto, A. Gonzalez-Prieto, and J. J. Aciego, "The evolution of model predictive control in multiphase electric drives: A growing field of research," *IEEE Ind. Electron. Mag.*, vol. 16, no. 4, pp. 29–39, Dec. 2022.

[14] A. Brosch, O. Wallscheid, and J. Böcker, "Torque and inductances estimation for finite model predictive control of highly utilized permanent magnet synchronous motors," *IEEE Trans. Ind. Informat.*, vol. 17, no. 12, pp. 8080–8091, May 2021.

[15] Z.-Q. Zhu, D. Liang, and K. Liu, "Online parameter estimation for permanent magnet synchronous machines: An overview," *IEEE Access*, vol. 9, pp. 59059–59084, 2021.

[16] B. Reddy, G. Poddar, and B. P. Muni, "Parameter estimation and online adaptation of rotor time constant for induction motor drive," *IEEE Trans. Ind. Appl.*, vol. 58, no. 2, pp. 1416–1428, Mar. 2022.

[17] U. Sengamalai, G. Anbazhagan, T. M. Thamizh Thentral, P. Vishnuram, T. Khurshaid, and S. Kamel, "Three phase induction motor drive: A systematic review on dynamic modeling, parameter estimation, and control schemes," *Energies*, vol. 15, no. 21, p. 8260, Nov. 2022.

[18] J. J. Aciego, I. Gonzalez Prieto, and M. J. Duran, "Model predictive control of six-phase induction motor drives using two virtual voltage vectors," *IEEE J. Emerg. Sel. Topics Power Electron.*, vol. 7, no. 1, pp. 321–330, Mar. 2019.

[19] I. Gonzalez-Prieto, M. J. Duran, M. Bermudez, F. Barrero, and C. Martin, "Assessment of virtual-voltage-based model predictive controllers in six-phase drives under open-phase faults," *IEEE J. Emerg. Sel. Topics Power Electron.*, vol. 8, no. 3, pp. 2634–2644, Sep. 2020.

[20] M. R. Arahal, F. Barrero, M. G. Satué, and D. R. Ramírez, "Predictive control of multi-phase motor for constant torque applications," *Machines*, vol. 10, no. 3, p. 211, Mar. 2022.

[21] O. Gonzalez, M. Ayala, C. Romero, L. Delorme, J. Rodas, R. Gregor, I. Gonzalez-Prieto, and M. J. Durán, "Model predictive current control of six-phase induction motor drives using virtual vectors and space vector modulation," *IEEE Trans. Power Electron.*, vol. 37, no. 7, pp. 7617–7628, Jul. 2022.

[22] M. Norambuena, P. Lezana, and J. Rodriguez, "A method to eliminate steady-state error of model predictive control in power electronics," *IEEE J. Emerg. Sel. Topics Power Electron.*, vol. 7, no. 4, pp. 2525–2530, Dec. 2019.

[23] A. Favato, P. G. Carlet, F. Toso, R. Torchio, and S. Bolognani, "Integral model predictive current control for synchronous motor drives," *IEEE Trans. Power Electron.*, vol. 36, no. 11, pp. 13293–13303, Nov. 2021.

[24] P. F. C. Gonçalves, S. M. A. Cruz, and A. M. S. Mendes, "Disturbance observer based predictive current control of six-phase permanent magnet synchronous machines for the mitigation of steady-state errors and current harmonics," *IEEE Trans. Ind. Electron.*, vol. 69, no. 1, pp. 130–140, Jan. 2022.

[25] I. Oliani, R. Figueiredo, L. F. N. Lourenço, A. Pelizari, and A. J. S. Filho, "Robust predictive current control using discrete-time integral action for induction motors," *IEEE J. Emerg. Sel. Topics Power Electron.*, vol. 11, no. 6, pp. 5766–5773, Dec. 2023.

[26] M. Ayala, J. Doval-Gandoy, J. Rodas, O. Gonzalez, R. Gregor, L. Delorme, C. Romero, and A. Fleitas, "Improving steady state accuracy in field-weakened six-phase induction machines with integrator and modulated predictive control," *Electronics*, vol. 13, no. 5, p. 952, Mar. 2024.

[27] M. S. Huang and C. M. Liaw, "Improved field-weakening control for IFO induction motor," *IEEE Trans. Aerosp. Electron. Syst.*, vol. 39, no. 2, pp. 647–659, Apr. 2003.

[28] M. Zaky, M. Khater, H. Yasin, and S. Shokralla, "Magnetizing inductance identification algorithm for operation of speed-sensorless induction motor drives in the field weakening region," in *Proc. MEPCON*, 2008, pp. 103–108.

[29] M. Ayala, J. Doval-Gandoy, J. Rodas, O. Gonzalez, R. Gregor, and M. Rivera, "A novel modulated model predictive control applied to six-phase induction motor drives," *IEEE Trans. Ind. Electron.*, vol. 68, no. 5, pp. 3672–3682, May 2021.

[30] Y. Zhao and T. Lipo, "Space vector PWM control of dual three-phase induction machine using vector space decomposition," *IEEE Trans. Ind. Electron.*, vol. 31, no. 5, pp. 1100–1109, May 1995.

[31] L. Harnefors, S. E. Saarakkala, and M. Hinkkanen, "Speed control of electrical drives using classical control methods," *IEEE Trans. Ind. Appl.*, vol. 49, no. 2, pp. 889–898, Mar. 2013.

[32] M. G. Satué, M. R. Arahal, M. G. Ortega, and D. R. Ramírez, "A simple rotor current estimation method for predictive control of multi-phase drives," *Int. J. Circuit Theory Appl.*, vol. 50, no. 12, pp. 4478–4491, Dec. 2022.

[33] C. Martín, M. R. Arahal, F. Barrero, and M. J. Durán, "Five-phase induction motor rotor current observer for finite control set model predictive control of stator current," *IEEE Trans. Ind. Electron.*, vol. 63, no. 7, pp. 4527–4538, Jul. 2016.

[34] J. Rodas, F. Barrero, M. R. Arahal, C. Martín, and R. Gregor, "Online estimation of rotor variables in predictive current controllers: A case study using five-phase induction machines," *IEEE Trans. Ind. Electron.*, vol. 63, no. 9, pp. 5348–5356, Sep. 2016.

[35] M. Novak, T. Dragicevic, and F. Blaabjerg, "Weighting factor design based on artificial neural network for finite set MPC operated 3L-NPC converter," in *Proc. IEEE Appl. Power Electron. Conf. Expo. (APEC)*, Mar. 2019, pp. 77–82.

[36] B. Majmunovic, T. Dragicevic, and F. Blaabjerg, "Multi objective modulated model predictive control of stand-alone voltage source converters," *IEEE J. Emerg. Sel. Topics Power Electron.*, vol. 8, no. 3, pp. 2559–2571, Sep. 2020.

[37] M. Ayala, J. Doval-Gandoy, J. Rodas, O. Gonzalez, R. Gregor, L. Delorme, C. Romero, and A. Fleitas, "Field-weakening strategy with modulated predictive current control applied to six-phase induction machines," *Machines*, vol. 12, no. 3, p. 178, Mar. 2024.
[38] S.-H. Kim and S.-K. Sul, "Maximum torque control of an induction machine in the field weakening region," *IEEE Trans. Ind. Appl.*, vol. 31, no. 4, pp. 787–794, Aug. 1995.
[39] L. Wang and L. Gan, "Integral FCS predictive current control of induction motor drive," *IFAC Proc. Volumes*, vol. 47, no. 3, pp. 11956–11961, 2014.
[40] J. A. Riveros, A. G. Yepes, F. Barrero, J. Doval-Gandoy, B. Bogado, O. Lopez, M. Jones, and E. Levi, "Parameter identification of multiphase induction machines with distributed windings—Part 2: Time-domain techniques," *IEEE Trans. Energy Convers.*, vol. 27, no. 4, pp. 1067–1077, Dec. 2012.
[41] G. I. Rivas-Martínez, J. Rodas, and J. D. Gandoy, "Statistical tools to evaluate the performance of current control strategies of power converters and drives," *IEEE Trans. Instrum. Meas.*, vol. 70, pp. 1–11, 2021.

MAGNO AYALA received the B.Eng. degree in electronic engineering from the Universidad Nacional de Asunción (UNA), Paraguay, in 2014, and the M.Sc. and Ph.D. degrees in power electronics from the Faculty of Engineering, UNA, in 2017 and 2020, respectively. His research interest includes control of multiphase ac machines. He received the 2020 Paraguayan National Science Award. He received an award from the Industrial Electronics Society, in 2021.

JESÚS DOVAL-GANDOY (Member, IEEE) received the M.Sc. degree from the Polytechnic University of Madrid, Madrid, Spain, in 1991, and the Ph.D. degree from the Universidad de Vigo, Vigo, Spain, in 1999. From 1991 to 1994, he worked in the industry. He is currently a Professor and the Head of the Applied Power Electronics Technology Research Group, Universidad de Vigo. His research interest includes ac power conversion.

JORGE RODAS (Senior Member, IEEE) received the Ph.D. degree through the Joint-University Program between the Universidad Nacional de Asunción (UNA) and the Universidad de Sevilla, in 2016. He is currently a Professor and the Research Director of the Facultad de Ingenieria, UNA. With over 120 published articles, his research focuses on advanced control applications for power electronic converters, renewable energy systems, and electric motor drives. He received the Paraguayan National Science Award.

OSVALDO GONZALEZ was born in Asunción, Paraguay. He received the B.Eng. degree in electronic engineering from the Universidad Nacional de Asunción (UNA), in 2014, and the M.Sc. and Ph.D. degrees in power electronics from the Faculty of Engineering, UNA, in 2017 and 2021, respectively. His research interest includes control of multiphase motors.

LARIZZA DELORME received the B.Eng. degree in electronic engineering from the Universidad Nacional de Asunción (UNA), Paraguay, in 2017, and the M.Sc. degree in electronic engineering with an emphasis on renewable energies and energy efficiency from the Universidad del Cono Sur de las Américas, in 2020. Her research interests include modeling, simulation, and control of multiphase drives.

PAOLA MAIDANA received the degree in electronic engineering and the Master of Science degree in power electronics from the Facultad de Ingeniería, Universidad Nacional de Asunción (UNA), Paraguay, where she is currently pursuing the Ph.D. degree in electronic engineering with the Power and Control Systems Laboratory (LSPyC). Her research interests include nonlinear control of electrical drives, multiphase induction machines, and power electronic converters.

CHRISTIAN MEDINA received the electronics engineering and Master of Science degrees in electronic engineering from the Facultad de Ingeniería, Universidad Nacional de Asunción, where he is currently pursuing the Ph.D. degree. His research interests include electronic power converters, nonlinear control, and induction machines.

RAÚL GREGOR received the bachelor's degree in electronic engineering from the Catholic University of Asunción, Paraguay, in 2005, and the M.Sc. and Ph.D. degrees in electronic, signal processing and communications from the University of Seville, Spain, in 2008 and 2010, respectively. He is currently the Head of the Laboratory of Power and Control System, Universidad Nacional de Asunción, Paraguay.